Crystal structure of ivermectin hemihydrate ethanolate, $(C_{48}H_{74}O_{14})(H_2O)_{0.5}(C_2H_5OH)_{0.82}$

James A. Kaduk,[1,2,a] Allison Tanis,[2] Alyssa Tovar,[2] Nicholas C. Boaz,[2] Amy M. Gindhart,[3] and Thomas N. Blanton[3]
[1]*Illinois Institute of Technology, 3101 S. Dearborn St., Chicago, Illinois 60616, USA*
[2]*North Central College, 131 S. Loomis St., Naperville, Illinois 60540, USA*
[3]*ICDD, 12 Campus Blvd., Newtown Square, Pennsylvania 19073-3273, USA*

(Received 30 January 2021; accepted 12 July 2021)

The crystal structure of ivermectin hemihydrate ethanolate has been solved and refined using synchrotron X-ray powder diffraction data and optimized using density functional techniques. Ivermectin hemihydrate ethanolate crystallizes in space group *C*2 (#5) with $a = 40.9374(10)$, $b = 9.26951(6)$, $c = 14.9488(2)$ Å, $\beta = 73.047(1)°$, $V = 5426.12(8)$ Å^3, and $Z = 4$. The structure consists of layers of ivermectin molecules parallel to the *bc*-plane. The water and ethanol molecules reside in small voids in the structure. The water molecule, the ethanol molecule, and hydroxyl groups act as donors in O–H···O hydrogen bonds. Several C–H···O hydrogen bonds were detected. The powder pattern has been submitted to ICDD for inclusion in the Powder Diffraction File™.
[doi:10.1017/S0885715621000488]

Key words: ivermectin, avermectin, Rietveld refinement, density functional theory

I. INTRODUCTION

Ivermectin (a type of avermectin; brand names Ivomec, Mectizan, Noromectin, Equivalan, and Stromectol) is a macrocyclic lactone derived from *Streptomyces avermitilis* with antiparasitic activity. It is used to treat head lice, scabies, river blindness, and other parasitic infections. Recently Ivermectin has been reviewed for application as a potential antiviral drug (Heidary and Gharebaghi, 2020). It is on the World Health Organization's List of Essential Medicines, which includes the most effective and safe medicines needed in a health system. It consists of not less than 80% of component B_{1a} and not more than 20% of component B_{1b} (Figure 1). In component B_{1a}, R = ethyl, and in component B_{1b}, R = methyl. In this study, the molecule is assumed to be component B_{1a}, as the smaller methyl group should fit into the crystallographic position of an ethyl group. The IUPAC name (CAS Registry number 70288-86-7) is (1*R*,4*S*,5′*S*,6*R*,6′*R*,8*R*,10*E*,12*S*,13*S*,14*E*,16*E*,20*R*,21*R*,24*S*)-6′-[(2*S*)-butan-2-yl]-21,24 -dihydroxy-12-[(2*R*,4*S*,5*S*,6*S*)-5-[(2*S*,4*S*,5*S*,6*S*)-5-hydroxy-4-methoxy-6-methyloxan-2 -yl]oxy-4-methoxy-6-methyloxan-2-yl]oxy-5′,11,13,22-tetramethylspiro[3,7,19-trioxatetracyclo[15.6.1.14,8.020,24]pentacosa-10,14,16,22-tetraene-6,2′-oxane]-2-one. The asymmetric unit of this structure is illustrated in Figure 2.

A powder pattern of ivermectin is reported in Rolim *et al.* (2014). Several apparent polymorphs of ivermectin have been characterized by X-ray powder diffraction and other analytical techniques, as reported in Grobler (2016).

This work was carried out as part of a project (Kaduk *et al.*, 2014) to determine the crystal structures of large-volume commercial pharmaceuticals and include high-quality powder diffraction data for these pharmaceuticals in the Powder Diffraction File (Gates-Rector and Blanton, 2019).

II. EXPERIMENTAL

The sample was a commercial reagent, purchased from United States Pharmacopeial Convention (USP) (Lot #R091C0), and was used as-received. The white powder was packed into a 1.5 mm diameter Kapton capillary and rotated during the measurement at ~50 Hz. The powder pattern was measured at 295 K at beamline 11-BM (Lee *et al.*, 2008; Wang *et al.*, 2008) of the Advanced Photon Source at Argonne National Laboratory using a wavelength of 0.412826 Å from 0.5° to 50° 2θ with a step size of 0.001° and a counting time of 0.1 s per step.

The pattern was indexed on a monoclinic unit cell with $a = 14.9487$, $b = 9.2704$, $c = 39.2623$ Å, $\beta = 94.379°$, and $V = 5425.08$ Å^3 using DICVOL14 (Louër and Boultif, 2014). Analysis of the systematic absences using EXPO2014 (Altomare *et al.*, 2013) suggested the space group *I*2. A reduced cell search in the Cambridge Structural Database (Groom *et al.*, 2016) yielded three hits, including Refcode BIFYOF (Seppala *et al.*, 2014), ivermectin acetone chloroform solvate, $C_{48}H_{74}O_{14}(C_3H_6O)_{0.5}(CHCl_3)$.

Refinement was carried out using GSAS-II (Toby and Von Dreele, 2013). Only the 1.0–20.0° portion of the pattern was included in the refinement ($d_{min} = 1.189$ Å). An initial refinement using the BIFYOF model did not fit the intensities particularly well, so the solvent molecules were removed from the model. A difference Fourier calculation yielded a peak at

[a]Author to whom correspondence should be addressed. Electronic mail: kaduk@polycrystallography.com

 0885-7156/2021/36(4)/247/10/$18.00

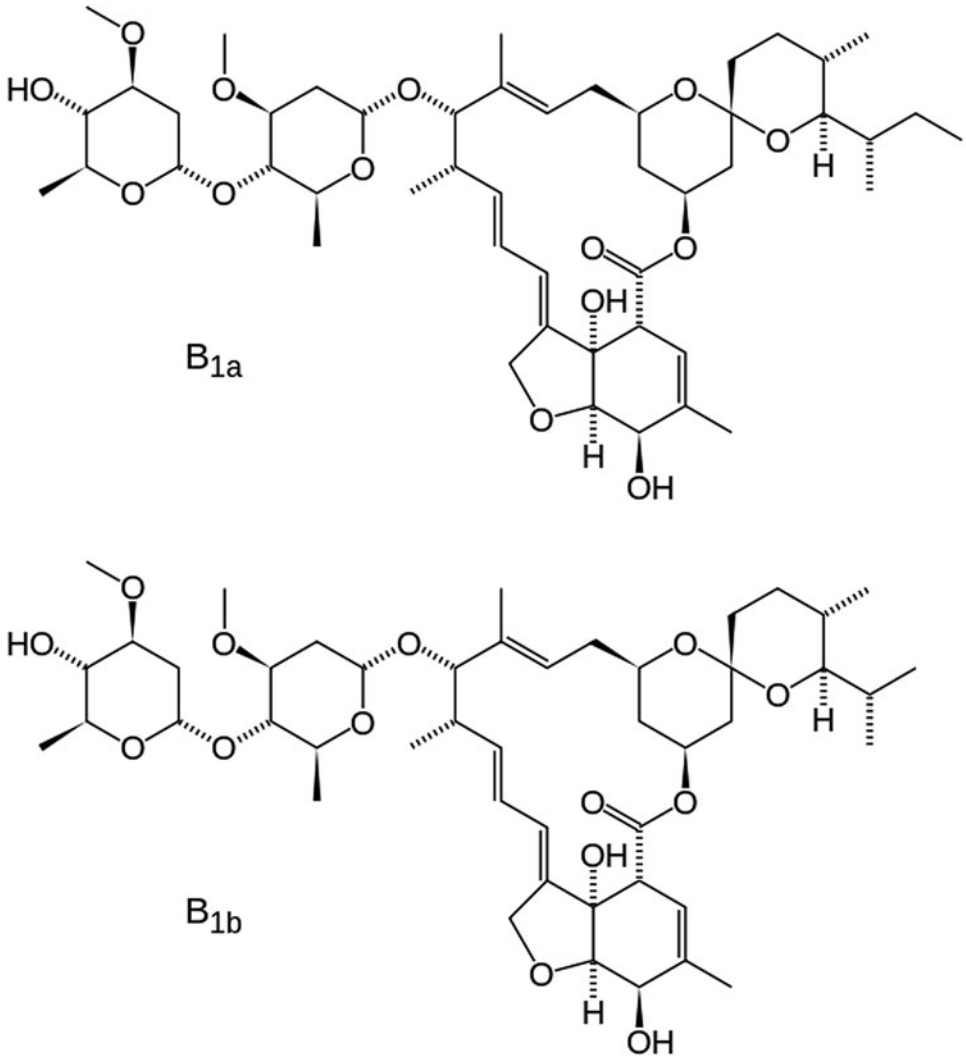

Figure 1. The molecular structures of forms B_{1a} and B_{1b} of ivermectin. The difference is an extra methyl group (C39 in our numbering) in form B_{1a}.

½, −0.1619,0, which was attributed to O147, the oxygen atom of a water molecule on a twofold axis.

Analysis of voids using Mercury (Macrae *et al.*, 2020) indicated the presence of a significant void, which was presumably occupied by some other solvated species.

The identity and amount of the solvated species occupying the void were shown to be ethanol using TGA and NMR spectroscopy. NMR spectroscopy was performed on a 400 MHz Bruker Avance Spectrometer equipped with a multi-nuclear probe. As shown in Figure 3, the NMR spectrum of the ivermectin sample in d_6-DMSO (10 mg in 0.5 ml of deutero solvent) indicates the presence of the methylene protons of ethanol at 3.34 ppm and the methyl protons of ethanol at 1.06 ppm. In both of these cases, the signals of the ethanol solvate are partially obscured by resonances from the pharmaceutical. Two-dimensional COSY NMR (^{1}H-^{1}H) of this sample indicate that the two putative ethanol signals are spin-correlated (Supplementary Figure S1). The addition of a small amount of pure ethanol led to an increase in intensity of both the methylene and methyl signals attributed to an ethanol solvate (Supplementary Figure S2). The ^{13}C NMR spectrum (Figure 4) of the ivermectin sample also indicated the presence of ethanol with the methyl and methylene group of this species exhibiting resonances at 57.12 and 19.05 ppm, respectively. The shifts in both the carbon and proton NMR spectra are consistent with literature values of ethanol in d_6DMSO (Gottlieb *et al.*, 1997). Moreover, an HSQC NMR spectrum indicates that the ^{1}H and ^{13}C NMR signals proposed to arise from ethanol are correlated (Supplementary Figure S3). The TGA analysis indicates a 6.03% weight loss from 144 to 156°C (Figure 5). The refined water/ethanol content corresponds to 5.07%. Since a real sample will contain some additional adsorbed surface species, the agreement is reasonable.

An ethanol molecule was inserted into the void using Materials Studio (Dassault, 2019), and the structure was optimized using the Forcite module. Refinement was re-started from this model. The *y*-coordinate of C2 was fixed to define the origin. All non-H bond distances and angles were subjected to restraints, based on a Mercury/Mogul Geometry Check (Bruno *et al.*, 2004; Sykes *et al.*, 2011) of the molecule. The results were exported to a .csv file. The Mogul average and standard deviation for each quantity were used as the restraint parameters, and were incorporated using the new feature Restraints/Edit Restraints/Add MOGUL Restraints, which reads the bond distance and angle restraints from the .csv file. The restraints contributed 11.2% to the final χ^2. The hydrogen atoms were included in calculated positions,

https://doi.org/10.1017/S0885715621000488 Published online by Cambridge University Press

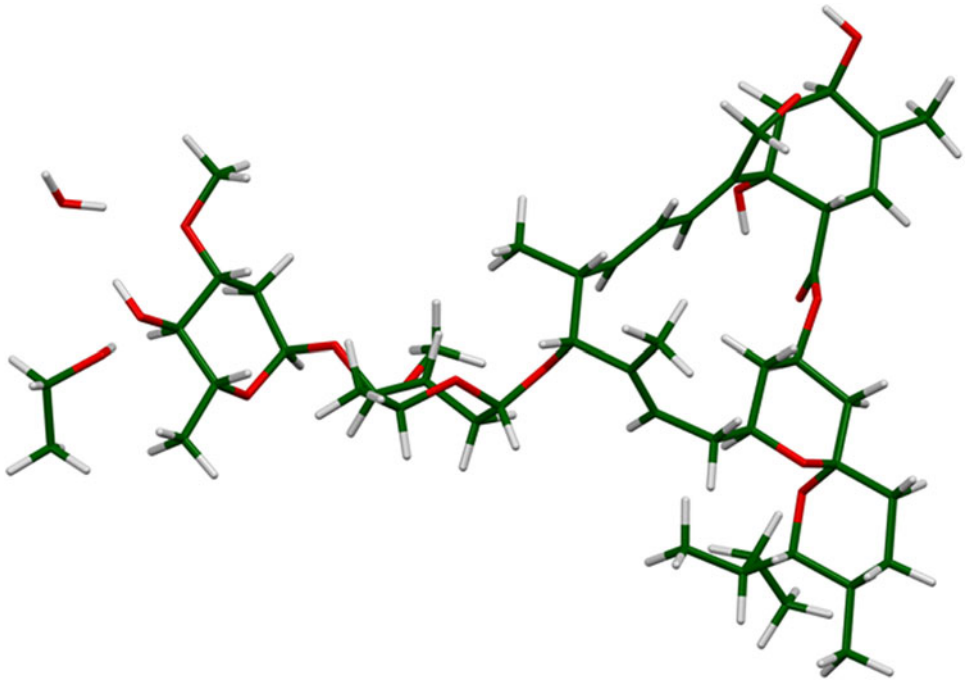

Figure 2. The asymmetric unit of ivermectin hemihydrate ethanolate.

which were recalculated during the refinement using Materials Studio (Dassault, 2019). Positions of the active hydrogens were derived by analysis of potential hydrogen bonding patterns. We did not attempt to refine the displacement coefficients in this very large structure. The U_{iso} of the heavy atoms were fixed at 0.05 Å^2, and those of the H atoms at 0.065 Å^2. It proved impossible to refine the generalize microstrain model and the atoms coordinates

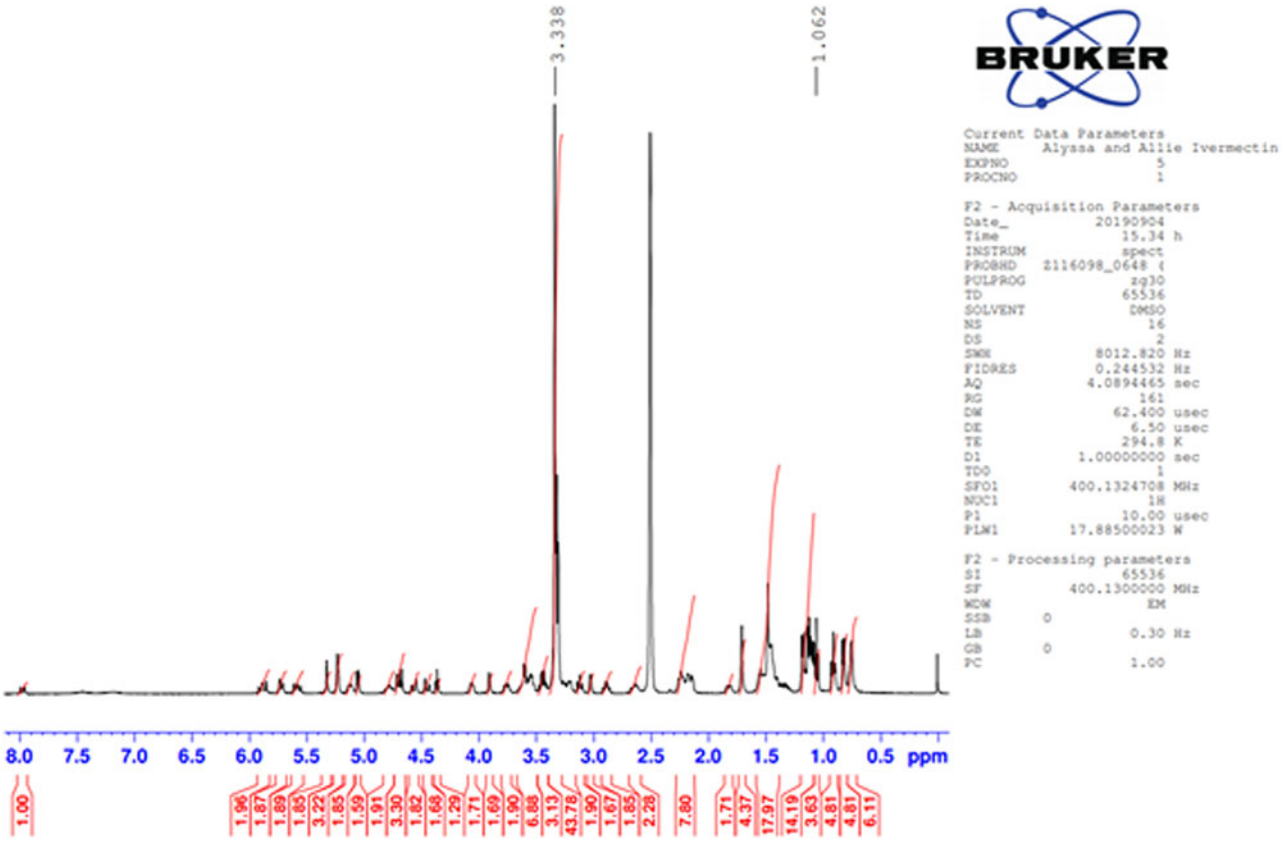

Figure 3. Proton NMR spectrum of ivermectin in d_6DMSO. Two signals from ethanol are found at 1.06 and 3.34 ppm. Note that the signal for the methylene at 3.34 ppm is overlapping with residual water and the methyl group at 1.06 ppm is overlapping with the pharmaceutical.

https://doi.org/10.1017/S0885715621000488 Published online by Cambridge University Press

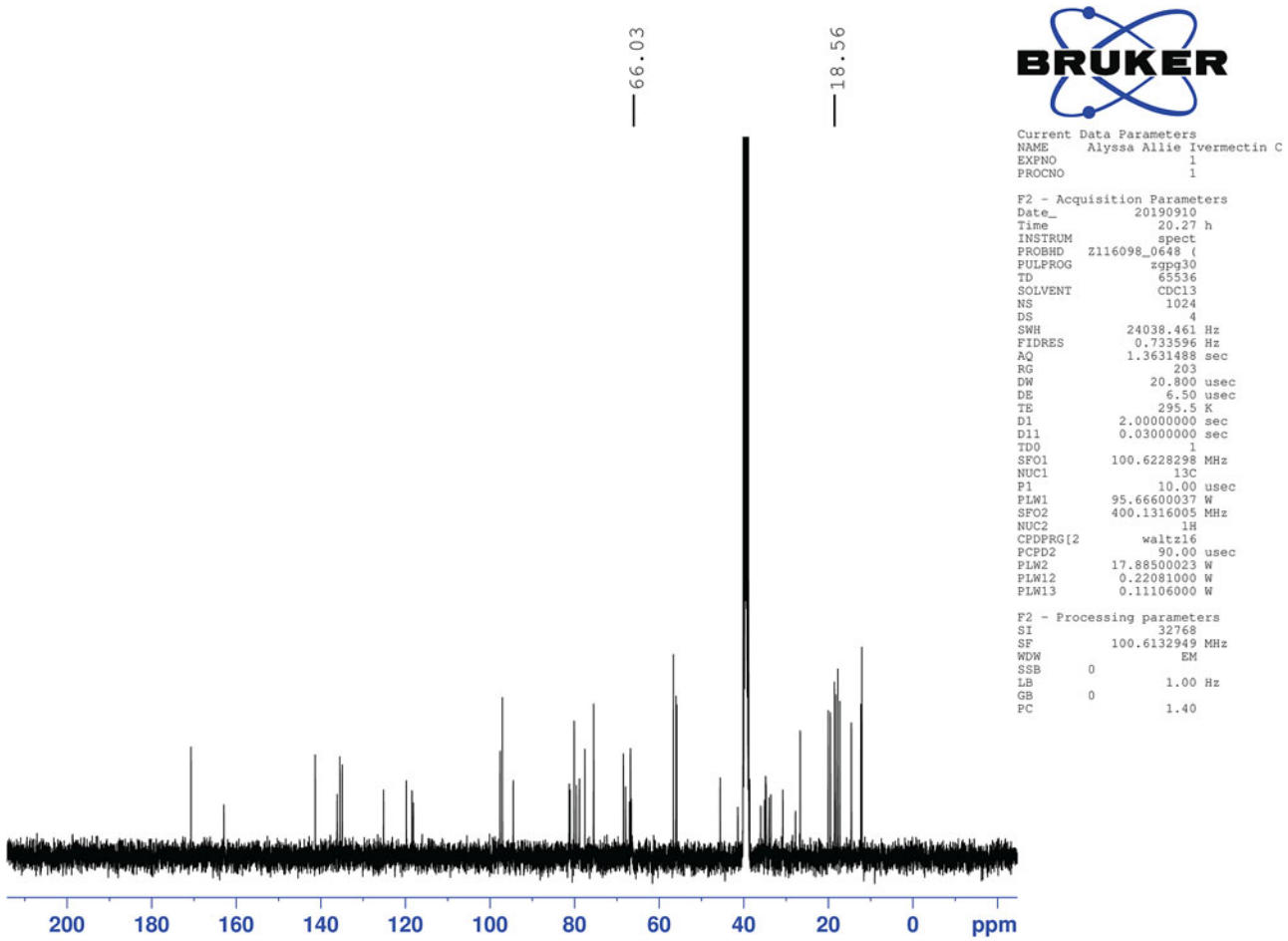

Figure 4. ^{13}C NMR spectrum of ivermectin in deuterated DMSO. The methyl and methylene group from ethanol gives rise to signals at 57.12 and 19.05 ppm, respectively.

simultaneously, so the profile terms were fixed in the final refinement. The background was modeled using a 3-term shifted Chebyshev polynomial and a 6-term diffuse scattering function, to describe the Kapton capillary and any amorphous component.

The model was converted from I2 to C2, because VASP is not able to work with I2. The final refinement (started from the result of the DFT calculation) of 204 variables using 19 031 observations and 173 restraints yielded the residuals R_{wp} = 0.1595 and GOF = 2.59. The largest peak (1.28 Å from C49) and hole (3.95 Å from C1) in the difference Fourier map were 0.40 and −0.40(10) eÅ^{-3}, respectively. The Rietveld plot is included as Figure 6. The largest errors in the fit are in the shapes and positions of some of the strong peaks, and may indicate subtle changes in the beam during the measurement. A Le Bail fit of the data yielded R_{wp} = 0.1208 and GOF = 1.95; the errors in the fit persist even in the absence of a structure model, indicating that the changes are real.

A density functional geometry optimization (fixed experimental unit cell) was started using VASP (Kresse and Furthmüller, 1996) through the MedeA graphical interface (Materials Design, 2016). The calculation was carried out on 16 2.4 GHz processors (each with 4 GB RAM) of a 64-processor HP Proliant DL580 Generation 7 Linux cluster at North Central College. The calculation used the GGA-PBE functional, a plane wave cutoff energy of 400.0 eV, and a k-point spacing of 0.5 Å^{-1} leading to a 3 × 3 × 1 mesh, and took ∼12.7 days. The DFT optimization was finished using CRYSTAL14 (Dovesi *et al.*, 2014). The basis sets for the H, C, and O atoms were those of Gatti *et al.* (1994). The calculation was run on eight 2.1 GHz Xeon cores (each with 6 GB RAM) of a 304-core Dell Linux cluster at IIT, using 8 k-points and the B3LYP functional, and took ∼8 days.

III. RESULTS AND DISCUSSION

The refined atom coordinates of ivermectin hemihydrate ethanolate and the coordinates from the DFT optimization are reported in the CIFs deposited with ICDD. The powder pattern of this study and that of Rolim *et al.* (2014) exhibit some similarities (Figure 7), but it is difficult to conclude that they represent the same material. Our pattern exhibits similarities to both Grobler's ivermectin starting material MG1 and his material crystallized from ethanol (MG6; Figure 8). The root-mean-square Cartesian displacement of the non-hydrogen atoms in the Rietveld-refined and DFT-optimized structures is 0.289 Å (Figure 9), within the range expected for correct structures (van de Streek and Neumann, 2014). This discussion concentrates on the DFT-optimized structure. The asymmetric unit (with atom numbering) is illustrated in Figure 10, and the crystal structure is presented in Figure 11.

The crystal structure is best viewed down the relatively-short b-axis (Figure 11). There are layers of

https://doi.org/10.1017/S0885715621000488 Published online by Cambridge University Press

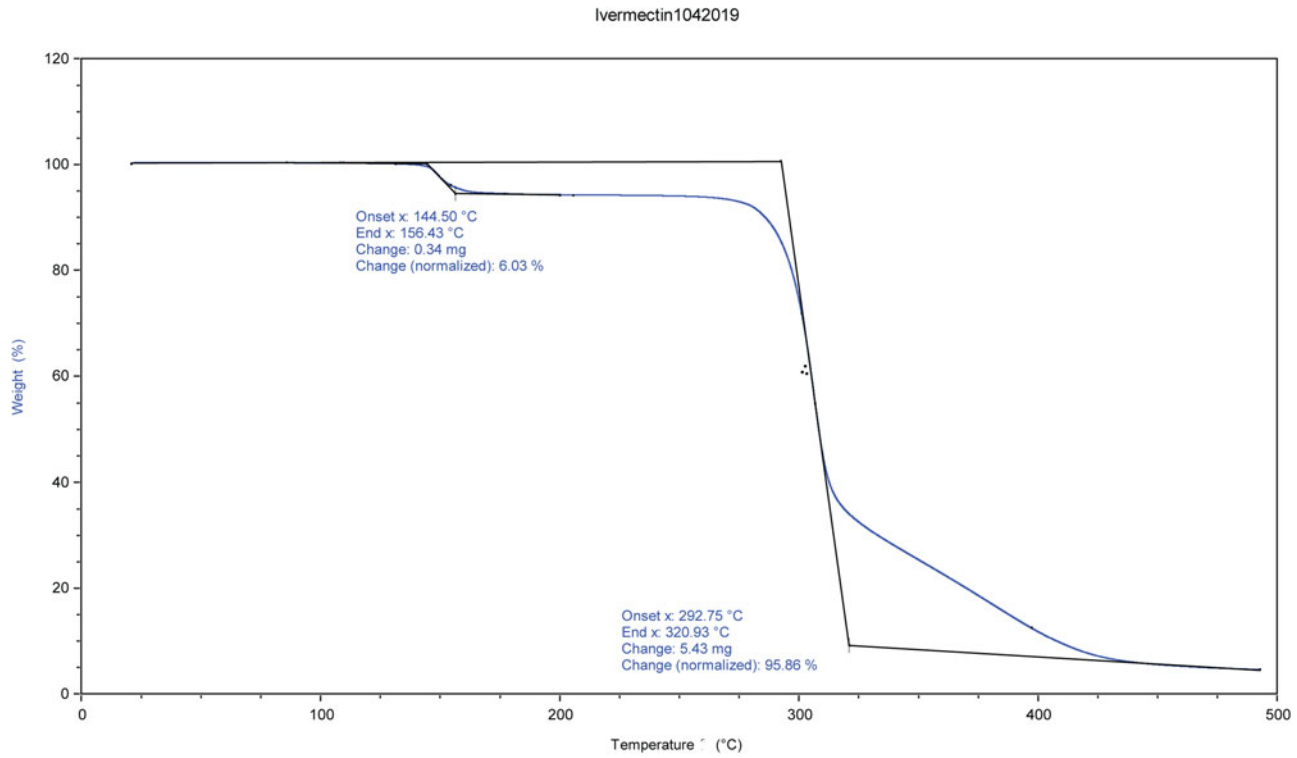

Figure 5. TGA analysis of ivermectin.

ivermectin molecules parallel to the *bc*-plane. The water and ethanol molecules reside in small voids in the structure (Figure 12; probe radius = 1.0 Å). One of the voids in Figure 12 appears to be empty; an attempt was made to place a water molecule in the void, but the occupancy refined to a negative value.

Almost all of the bond distances, angles, and torsion angles fall within the normal ranges indicated by a Mercury/Mogul Geometry check (Macrae *et al.*, 2020). The O57–C28–C30 angle of 109.3° (average = 105.8(10)°, *Z*-score = 3.6) is flagged as unusual. This angle lies slightly outside a narrow distribution of a few similar angles. The torsion angle C9–O54–C11–C12 is flagged as unusual; this represents the linking of the two portions of the molecule, and it is likely that crystal packing forces influence the molecular conformation. The torsion angles involving rotation around the

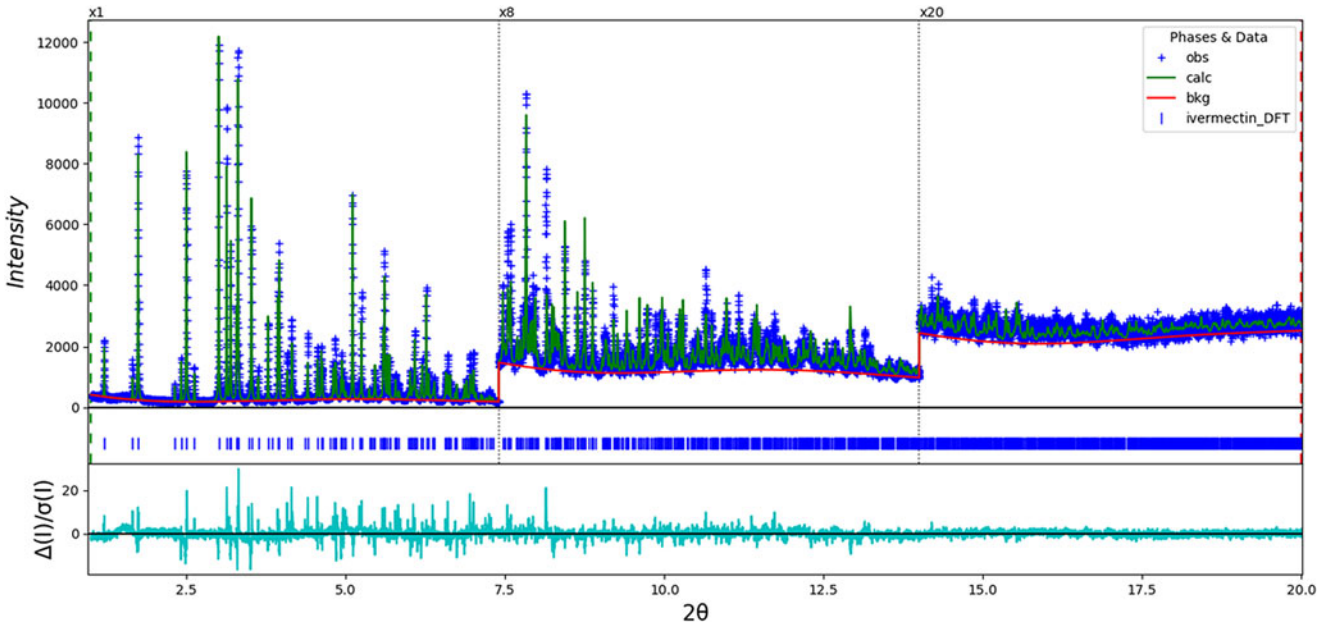

Figure 6. The Rietveld plot for the refinement of ivermectin hemihydrate ethanolate. The blue crosses represent the observed data points, and the green line is the calculated pattern. The cyan curve is the normalized error plot. The vertical scale has been multiplied by a factor of 8× for $2\theta > 7.4°$, and by a factor of 20× for $2\theta > 14.0°$.

https://doi.org/10.1017/S0885715621000488 Published online by Cambridge University Press

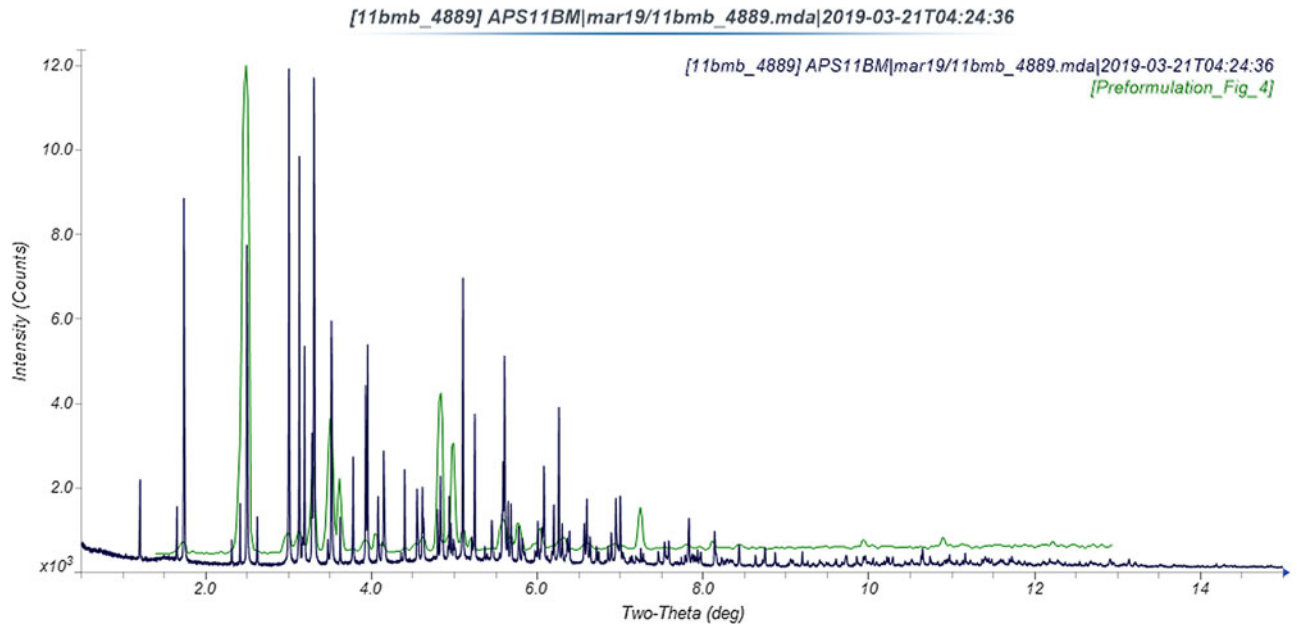

Figure 7. Comparison of the synchrotron pattern of ivermectin hemihydrate ethanolate to the diffraction pattern reported by Rolim *et al.* (2014). The published pattern was digitized using UN-SCAN-IT (Silk Scientific, 2013) and scaled to the synchrotron wavelength of 0.412826 Å using MDI JADE Pro (MDI, 2019).

C37–C38 bond (such as C33–C37–C38–C39) are flagged as unusual. This angle lies near a minor *gauche* population of mainly *trans* angles.

Quantum chemical geometry optimization of the ivermectin molecule (DFT/B3LYP/6-31G*/water) using Spartan '18 (Wavefunction, 2019) indicated that the observed solid-state conformation is 12.9 kcal mol^{-1} higher in energy than the local minimum (Figure 13). The rms Cartesian displacement between the two structures is 0.547 Å, and the displacements are spread throughout the molecule. Molecular mechanics conformational analysis (MMFF) indicated that the observed conformation is essentially the global minimum-energy conformation.

Analysis of the contributions to the total crystal energy using the Forcite module of Materials Studio (Dassault, 2019) suggests that bond, angle, and torsion contributions to the intramolecular deformation energy are significant. The intermolecular energy is dominated by electrostatic attractions, which in this force-field-based analysis include cation coordination and hydrogen bonds. The hydrogen bonds are better analyzed using the results of the DFT calculation.

Hydrogen bonds are significant in the crystal structure (Table I). The water molecule O147–H146 acts as a donor to the hydroxyl group O63. The ethanol molecule acts as a donor to the hydroxyl group O60. The hydroxyl group O63–H138 makes bifurcated hydrogen bonds to the ketone

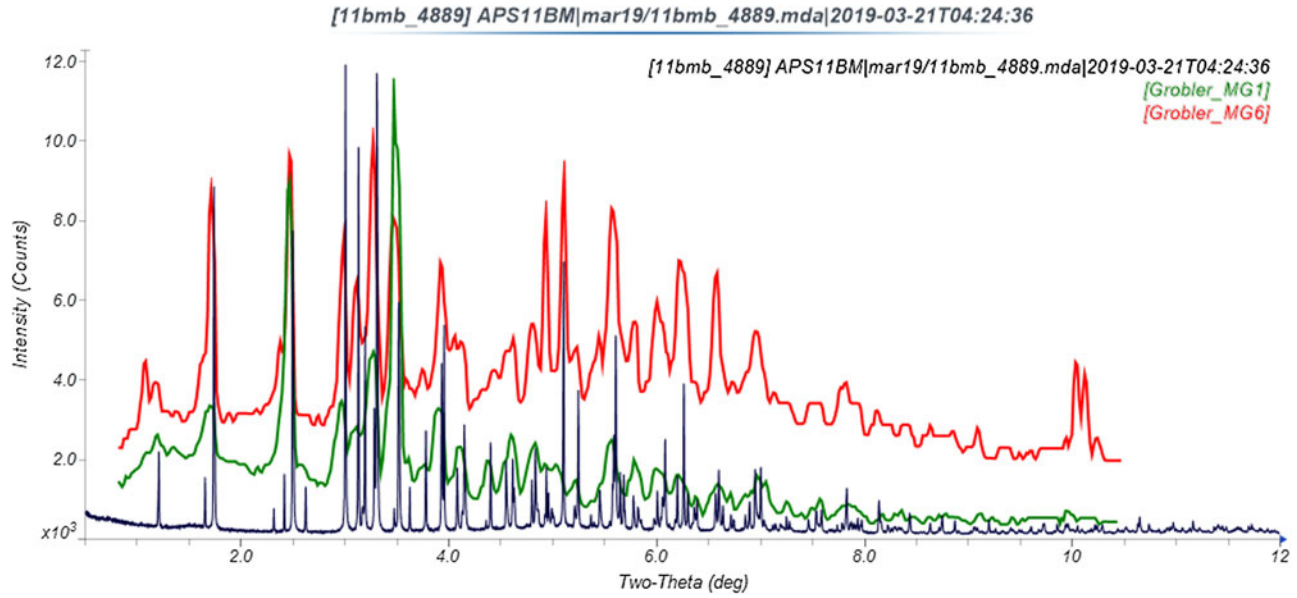

Figure 8. Comparison of the synchrotron pattern of ivermectin hemihydrate ethanolate to diffraction patterns of Forms MG1 and MG6 reported by Grobler (2016). The published patterns were digitized using UN-SCAN-IT (Silk Scientific, 2013) and scaled to the synchrotron wavelength of 0.412826 Å Using MDI JADE Pro (MDI, 2019).

https://doi.org/10.1017/S0885715621000488 Published online by Cambridge University Press

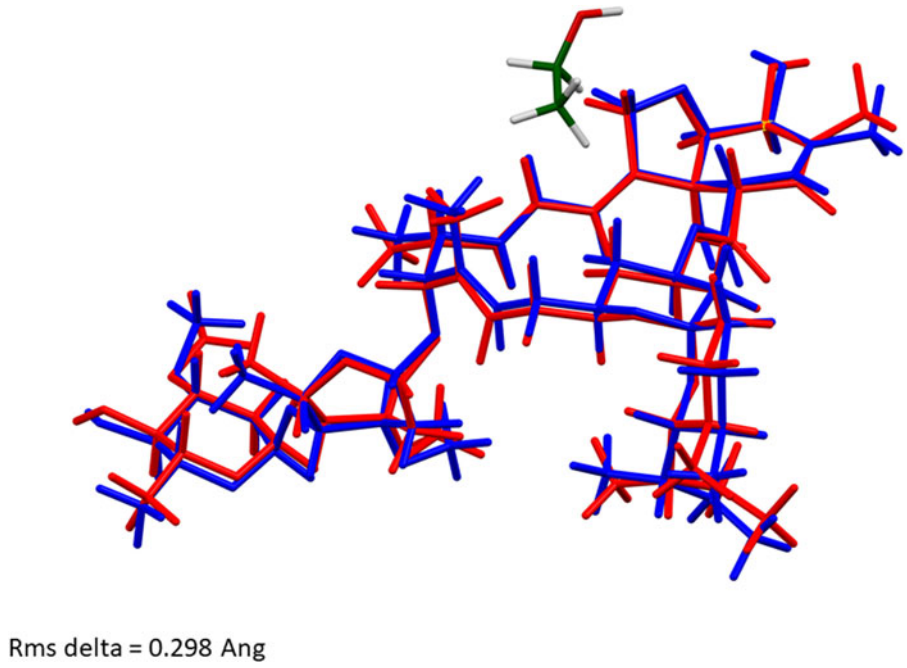

Figure 9. Comparison of the Rietveld-refined (red) and VASP-optimized (blue) structures of ivermectin. The rms Cartesian displacement is 0.298 Å.

O64 and the hydroxyl group O60. The hydroxyl group O62–H137 acts as a donor to the ether oxygen O55. The hydroxyl group O60–H136 acts as a donor to the ether oxygen O59. Some of these H-bonds are intramolecular. The energies of the O–H···O hydrogen bonds were calculated from the correlation of Rammohan and Kaduk (2018). Several C–H···O

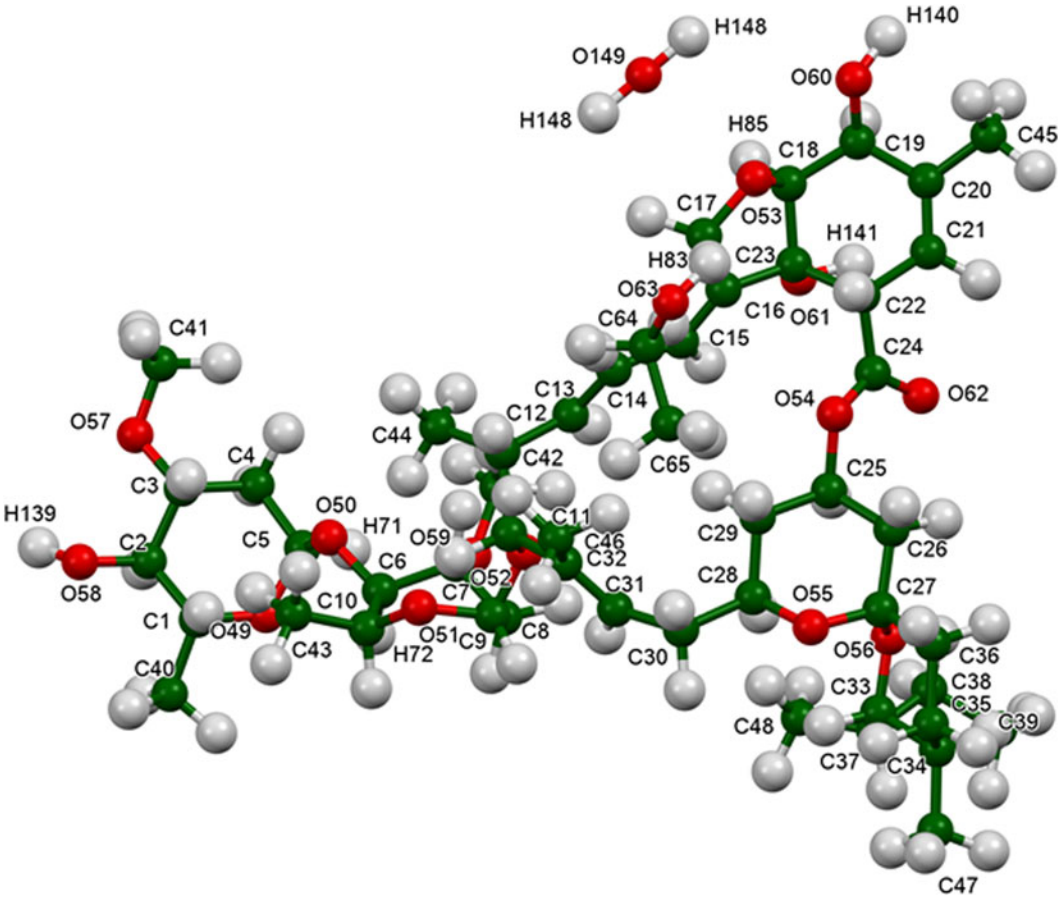

Figure 10. The asymmetric unit of ivermectin hemihydrate ethanolate, with the atom numbering. The atoms are represented by 50% probability spheroids. The U_{iso} were not refined, but assigned as the "reasonable" values of 0.05 Å^2 for the heavy atoms and 0.065 Å^2 for the hydrogen atoms.

https://doi.org/10.1017/S0885715621000488 Published online by Cambridge University Press

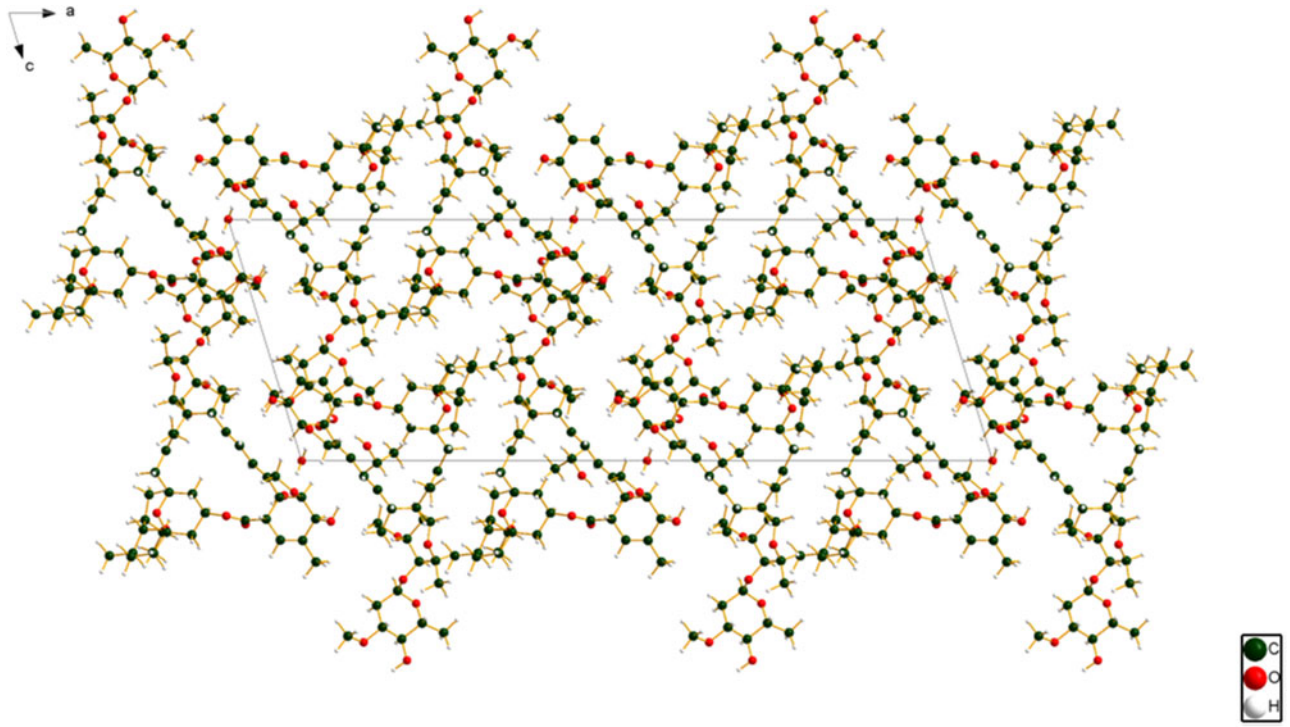

Figure 11. The crystal structure of ivermectin hemihydrate ethanolate, viewed down the *b*-axis.

hydrogen bonds were detected. Although weak, their number means that they probably contribute significantly to the crystal energy.

The volume enclosed by the Hirshfeld surface (Figure 14; Hirshfeld, 1977; Turner *et al.*, 2017) is 1359.03 Å^3, 100.19% of one-fourth the unit cell volume. The molecules are thus tightly packed. All of the significant close contacts (red in Figure 14) involve the hydrogen bonds. The volume/non-hydrogen atom is 19.2 Å^3.

The Bravais–Friedel–Donnay–Harker (Bravais, 1866; Friedel, 1907; Donnay and Harker, 1937) morphology suggests that we might expect platy morphology for ivermectin hemihydrate ethanolate, with {100} as the principal faces. A second-order spherical harmonic model for preferred orientation was incorporated into the refinement. The texture index was only 1.007, indicating that preferred orientation was not significant in this rotated capillary specimen. The powder pattern of ivermectin hemihydrate ethanolate from this synchrotron data set has been submitted to ICDD for inclusion in the Powder Diffraction File™.

IV. DEPOSITED DATA

The Crystallographic Information Framework (CIF) files containing the results of the Rietveld refinement (including the raw data) and the DFT geometry optimization were deposited with the ICDD. The data can be requested at info@icdd.

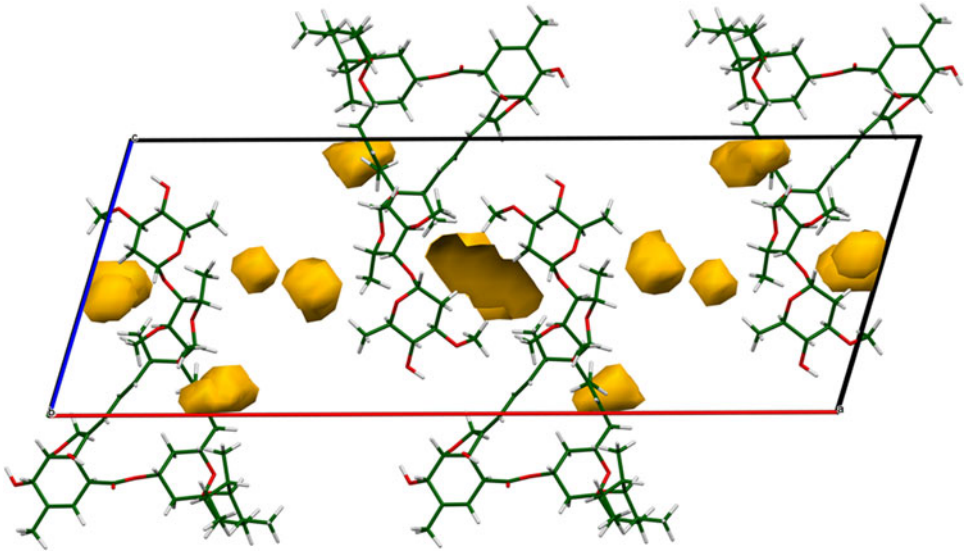

Figure 12. The voids (probe radius = 1.0 Å) in the structure of ivermectin hemihydrate ethanolate. The water and ethanol molecules reside in these voids.

https://doi.org/10.1017/S0885715621000488 Published online by Cambridge University Press

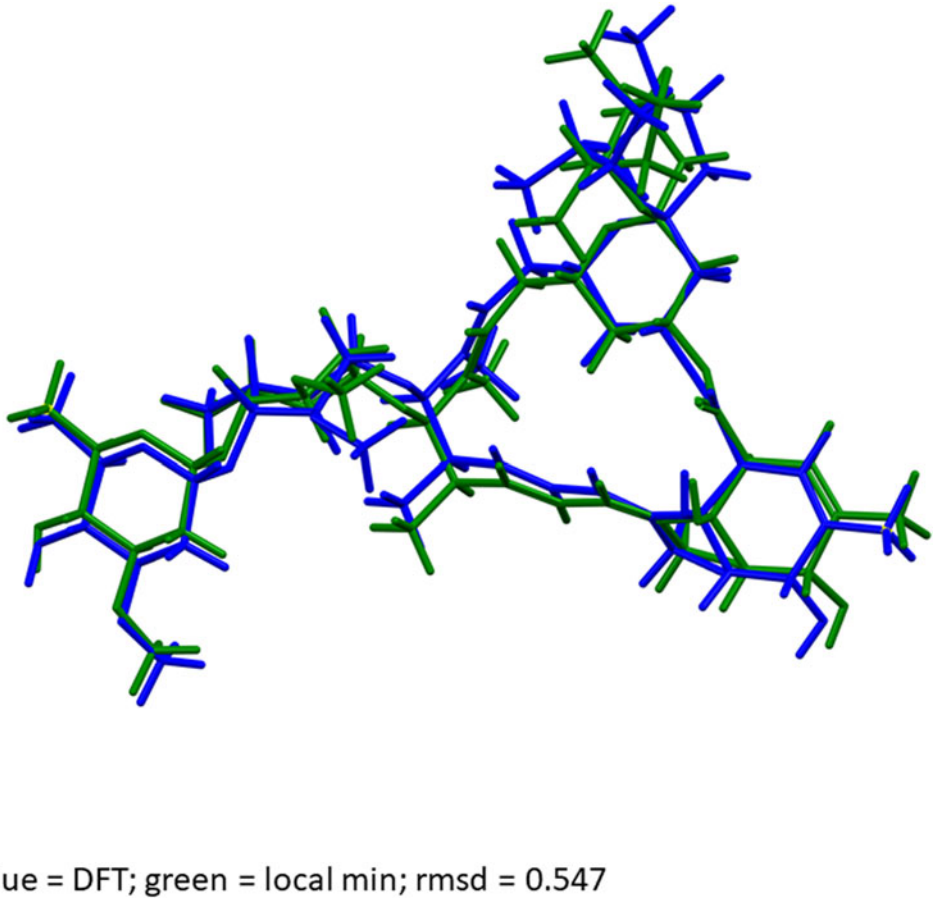

Figure 13. Comparison of the observed solid-state ivermectin conformation (blue) to the local minimum-energy conformation. The rms Cartesian displacement is 0.547 Å, and the energy difference is 12.9 kcal mol^{-1}.

com. The three Supplementary Figures have been deposited with Cambridge University Press.

SUPPLEMENTARY MATERIAL

The supplementary material for this article can be found at https://doi.org/10.1017/S0885715621000488.

ACKNOWLEDGEMENTS

The use of the Advanced Photon Source at Argonne National Laboratory was supported by the U.S. Department of Energy, Office of Science, Office of Basic Energy Sciences, under Contract No. DE-AC02-06CH11357. This work was partially supported by the International Centre for Diffraction Data. We thank Lynn Ribaud

TABLE I. Hydrogen bonds (CRYSTAL14) in ivermectin hemihydrate ethanolate.

H-bond	D-H (Å)	H···A (Å)	D···A (Å)	D-H···A (°)	Overlap (*e*)	*E* (kcal mol^{-1})
O147–H146···O63	0.973	1.967	2.912	170.9	0.041	11.1
O65–H140···O60	0.974	1.883	2.822	166.6	0.042	11.2
O63–H138···O64	0.975	2.046[a]	2.875	139.2	0.032	9.8
O63–H138···O60	0.975	2.276	2.981	126.3	0.022	8.1
O62–H137···O55	0.969	2.201[a]	2.801	80.6	0.018	7.3
O60–H136···O59	0.973	2.330[a]	2.788	101.7	0.021	7.9
C47–H132···O53	1.091	2.561	3.647	140.3	0.015	
C40–H111···O56	1.094	2.726	3.718	161.3	0.010	
C38–H104···O58	1.095	2.388	2.897	105.2	0.014	
C33–H97···O57	1.101	2.474	2.937	100.0	0.014	
C31–H96···O54	1.089	2.367	2.817	101.9	0.017	
C28–H91···O58	1.096	2.351	2.867	100.3	0.012	
C6–H72···O51	1.096	2.556[a]	2.956	101.3	0.011	
C5–H71···O61	1.094	2.467[a]	3.219	121.4	0.016	
C2–H67···O55	1.096	2.457	3.159	139.4	0.015	
C1–H66···O64	1.093	2.430	3.353	134.0	0.010	
C1–H66···O52	1.093	2.631[a]	2.971	96.9	0.010	

[a]Intramolecular.

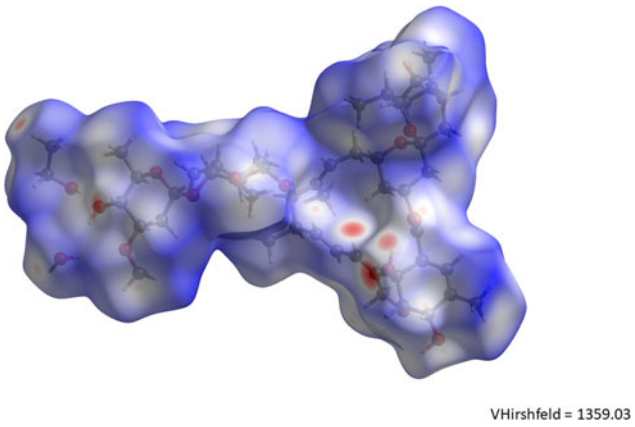

Figure 14. The Hirshfeld surface of ivermectin hemihydrate ethanolate. Intermolecular contacts longer than the sums of the van der Waals radii are colored blue, and contacts shorter than the sums of the radii are colored red. Contacts equal to the sums of radii are white.

and Saul Lapidus for their assistance in the data collection, and Andrey Rogachev for the use of computing resources at IIT.

CONFLICTS OF INTEREST

The authors have no conflicts of interest to declare.

Altomare, A., Cuocci, C., Giacovazzo, C., Moliterni, A., Rizzi, R., Corriero, N., and Falcicchio, A. (**2013**). "EXPO2013: a kit of tools for phasing crystal structures from powder data," J. Appl. Crystallogr. **46**, 1231–1235.

Bravais, A. (**1866**). *Etudes Cristallographiques* (Gauthier Villars, Paris).

Bruno, I. J., Cole, J. C., Kessler, M., Luo, J., Motherwell, W. D. S., Purkis, L. H., Smith, B. R., Taylor, R., Cooper, R. I., Harris, S. E., and Orpen, A. G. (**2004**). "Retrieval of crystallographically-derived molecular geometry information," J. Chem. Inf. Sci. **44**, 2133–2144.

Dassault Systèmes (**2019**). *Materials Studio 2019* (BIOVIA, San Diego, CA).

Donnay, J. D. H. and Harker, D. (**1937**). "A new law of crystal morphology extending the law of Bravais," Am. Mineral. **22**, 446–447.

Dovesi, R., Orlando, R., Erba, A., Zicovich-Wilson, C. M., Civalleri, B., Casassa, S., Maschio, L., Ferrabone, M., De La Pierre, M., D-Arco, P., Noël, Y., Causà, M., and Kirtman, B. (**2014**). "CRYSTAL14: a program for the ab initio investigation of crystalline solids," Int. J. Quantum Chem. **114**, 1287–1317.

Friedel, G. (**1907**). "Etudes sur la loi de Bravais," Bull. Soc. Fr. Mineral. **30**, 326–455.

Gates-Rector, S. and Blanton, T. N. (**2019**). "The Powder Diffraction File: a quality materials characterization database," Powder Diffr. **34**(4), 352–260.

Gatti, C., Saunders, V. R., and Roetti, C. (**1994**). "Crystal-field effects on the topological properties of the electron-density in molecular crystals - the case of urea," J. Chem. Phys. **101**, 10686–10696.

Gottlieb, H. E., Kotlyar, V., and Nudelman, A. (**1997**). "NMR chemical shifts of common laboratory solvents as trace impurities," J. Org. Chem. **62**, 7512–7515.

Grobler, M. L. J. (**2016**). "Crystal polymorphism and pseudopolymorphism of ivermectin," Master's Thesis, North-West University, Potchefstroom, South Africa.

Groom, C. R., Bruno, I. J., Lightfoot, M. P., and Ward, S. C. (**2016**). "The Cambridge Structural Database," Acta Crystallogr. Sect. B: Struct. Sci., Cryst. Eng. Mater. **72**, 171–179.

Heidary, F. and Gharebaghi, R. (**2020**). "Ivermectin: a systematic review from antiviral effects to COVID-19 complimentary regimen," J. Antibiotics **73**, 593–602.

Hirshfeld, F. L. (**1977**). "Bonded-atom fragments for describing molecular charge densities," Theor. Chem. Acta **44**, 129–138.

Kaduk, J. A., Crowder, C. E., Zhong, K., Fawcett, T. G., and Suchomel, M. R. (**2014**). "Crystal structure of atomoxetine hydrochloride (Strattera), $C_{17}H_{22}NOCl$," Powder Diffr. **29**(3), 269–273.

Kresse, G. and Furthmüller, J. (**1996**). "Efficiency of ab-initio total energy calculations for metals and semiconductors using a plane-wave basis set," Comput. Mater. Sci. **6**, 15–50.

Lee, P. L., Shu, D., Ramanathan, M., Preissner, C., Wang, J, Beno, M. A., Von Dreele, R. B., Ribaud, L., Kurtz, C, Antao, S. M., Jiao, X., and Toby, B. H. (**2008**). "A twelve-analyzer detector system for high-resolution powder diffraction," J. Synch. Rad. **15**(5), 427–432.

Louër, D. and Boultif, A. (**2014**). "Some further considerations in powder diffraction pattern indexing with the dichotomy method," Powder Diffr. **29**, S7–S12.

Macrae, C. F., Sovago, I., Cottrell, S. J., Galek, P. T. A., McCabe, P., Pidcock, E., Platings, M., Shields, G. P., Stevens, J. S., Towler, M., and Wood, P. A. (**2020**). "*Mercury 4.0*; from visualization to design and prediction," J. Appl. Crystallogr. **53**, 226–235.

Materials Design (**2016**). *MedeA 2.20.4* (Materials Design Inc., Angel Fire, NM).

MDI (**2019**). MDI JADE Pro Version 7.7 (Materials Data, Livermore, CA).

Rammohan, A. and Kaduk, J. A. (**2018**). "Crystal structures of alkali metal (Group 1) citrate salts," Acta Crystallogr. Sect. B: Cryst. Eng. Mater. **74**, 239–252. doi:10.1107/S2052520618002330.

Rolim, L. A., do Santos, F. C. M., Chaves, L. L., Goncalves, M. L. C. M., Freitas-Neto, J. L., do Nascimento, A. L. d. S., Soares-Sobrinho, J. L., de Albuquerque, M. M., de Lima, M. d. C. A., and Rolim-Neto, P. J. (**2014**). "Preformulation study of ivermectin raw material," J. Therm. Anal. Calorim. doi:10.1007/s10973-014-3691-9.

Seppala, E., Kolehmainen, E., Osmialowski, B., and Gawinecki, R. (**2014**). CSD Communication; Refcode BIFYOF.

Silk Scientific (**2013**). *UN-SCAN-IT 7.0* (Silk Scientific Corporation, Orem, UT).

Sykes, R. A., McCabe, P., Allen, F. H., Battle, G. M., Bruno, I. J., and Wood, P. A. (**2011**). "New software for statistical analysis of Cambridge Structural Database data," J. Appl. Crystallogr. **44**, 882–886.

Toby, B. H. and Von Dreele, R. B. (**2013**). "GSAS II: the genesis of a modern open source all purpose crystallography software package," J. Appl. Crystallogr. **46**, 544–549.

Turner, M. J., McKinnon, J. J., Wolff, S. K., Grimwood, D. J., Spackman, P. R., Jayatilaka, D., and Spackman, M. A. (**2017**). CrystalExplorer17 (University of Western Australia). Available at: http://hirshfeldsurface.net.

van de Streek, J. and Neumann, M. A. (**2014**). "Validation of molecular crystal structures from powder diffraction data with dispersion-corrected density functional theory (DFT-D)," Acta Crystallogr. Sect. B: Struct. Sci., Cryst. Eng. Mater. **70**(6), 1020–1032.

Wang, J., Toby, B. H., Lee, P. L., Ribaud, L., Antao, S. M., Kurtz, C., Ramanathan, M., Von Dreele, R. B., and Beno, M. A. (**2008**). "A dedicated powder diffraction beamline at the advanced photon source: commissioning and early operational results," Rev. Sci. Inst. **79**, 085105.

Wavefunction, Inc. (**2019**). Spartan '18 Version 1.4.4, Wavefunction Inc., 18401 Von Karman Ave., Suite 370, Irvine, CA 92612.